Nonlinear Unmixing by Using Different Metrics in a Linear Unmixing Chain

Rob Heylen, Paul Scheunders, Anand Rangarajan, and Paul Gader

***Abstract*—Several popular endmember extraction and unmixing algorithms are based on the geometrical interpretation of the linear mixing model, and assume the presence of pure pixels in the data. These endmembers can be identified by maximizing a simplex volume, or finding maximal distances in subsequent subspace projections, while unmixing can be considered a simplex projection problem. Since many of these algorithms can be written in terms of distance geometry, where mutual distances are the properties of interest instead of Euclidean coordinates, one can design an unmixing chain where other distance metrics are used. Many preprocessing steps such as (nonlinear) dimensionality reduction or data whitening, and several nonlinear unmixing models such as the Hapke and bilinear models, can be considered as transformations to a different data space, with a corresponding metric. In this paper, we show how one can use different metrics in geometry-based endmember extraction and unmixing algorithms, and demonstrate the results for some well-known metrics, such as the Mahalanobis distance, the Hapke model for intimate mixing, the polynomial post-nonlinear model, and graph-geodesic distances. This offers a flexible processing chain, where many models and preprocessing steps can be transparently incorporated through the use of the proper distance function.**

***Index Terms*—Hyperspectral imaging, spectral analysis.**

I. Introduction

HYPERSPECTRAL unmixing [1] concerns the decomposition of a single spectrum, observed in a pixel of a hyperspectral image, into its constituent components, called endmembers. Each of these endmembers has an associated abundance, and depending on the model used, several constraints are typically imposed on these endmembers and abundances.

The most popular model for describing the spectral mixing observed in a hyperspectral image is the linear mixing model (LMM). This model assumes that an observed spectrum $\boldsymbol{x}_n \in \mathbb{R}^D$ is a linear combination of M endmember spectra $\{\boldsymbol{e}_m\}_{m=1}^M$, with corresponding abundances that are positive and sum to one

$$\boldsymbol{x}_n = \sum_{m=1}^{M} a_{nm}\boldsymbol{e}_m + \boldsymbol{\eta}_n$$
$$\forall n, m : a_{nm} \geq 0, \quad \sum_m a_{nm} = 1. \tag{1}$$

Manuscript received July 31, 2014; revised October 24, 2014; accepted November 22, 2014. Date of publication December 17, 2014; date of current version July 30, 2015.

R. Heylen and P. Scheunders are with IMinds—Vision Laboratory, University of Antwerp, 2610 Antwerp, Belgium (e-mail: rob.heylen/paul.scheunders@uantwerpen.com).

A. Rangarajan and P. Gader are with CISE, University of Florida, Gainesville, FL 32611 USA (e-mail: pgader/anand@cise.ufl.edu).

Color versions of one or more of the figures in this paper are available online at http://ieeexplore.ieee.org.

Digital Object Identifier 10.1109/JSTARS.2014.2375342

The term $\boldsymbol{\eta}_n$ describes noise and is typically assumed to be uncorrelated Gaussian noise. With the constraints on the abundances, the LMM has a clear geometrical interpretation. The allowed pixel values lie in the convex set spanned by the endmembers, which is a simplex in the high-dimensional spectral space.

In hyperspectral unmixing applications, one usually assumes that the endmembers and the abundances are unknown, and have to be derived from the data. While approaches exist that try to estimate both the endmember and abundance matrix simultaneously, such as nonnegative matrix factorization, most algorithms for unmixing employ a two-step strategy. The first step is to extract the endmembers from the data using an endmember extraction algorithm (EEA), followed by a second step that solves the inversion problem to determine the corresponding abundances. Several of these EEAs look for the endmembers in the data itself, implicitly assuming that pure pixels exist for each endmember, i.e., pixels that contain only a single endmember component.

This pure pixel assumption, together with the geometrical interpretation of the LMM, has led to several EEAs trying to find the spanning vertices of the simplex in spectral space. The NfindR algorithm [2], for instance, tries to find the largest volume simplex in the data set by starting from a randomly chosen initial simplex, and iteratively updating simplex vertices until no larger simplex can be found. The data points spanning this simplex are assigned as endmembers. NfindR has been shown to yield results comparable to many other EEAs [3], but is computationally very intensive, suffers from inconsistent results due to the random initialization and updating, can get stuck in local minima, and is generally slow. The NfindR algorithm has been studied extensively, however, and many recent results have appeared on the updating strategy employed in the NfindR algorithm [4]–[6], the initialization of the algorithm [4], [6]–[8], the analytics [9], and GPU implementation [10]. Although the NfindR algorithm is generally much slower than many other EEAs, it is still under active development and used in many unmixing chains.

An alternative to the NfindR algorithm that works much faster is the maximum distance (MaxD) algorithm [11]. Here, one assumes first that the pixels with smallest and largest magnitude (ℓ_2-norm) are endmembers. Then, one iteratively adds endmembers by orthogonal projection onto the subspace orthogonal to the hyperplane through the endmembers already selected, and locating the pixel with largest magnitude. This is again repeated until all endmembers have been extracted. The same idea was exploited in several other algorithms, such as the automated target generation process (ATGP) algorithm [12]

and the popular vertex component analysis (VCA) algorithm [13]. A similar idea of using orthogonal subspace projections to identify endmembers was employed in [14].

Another EEA based on geometrical principles and the pure pixel assumption is the simplex growing algorithm (SGA) [15]. In the SGA, one first selects an initial endmember with an endmember initialization algorithm and then iteratively adds endmembers by identifying which one will yield the maximal simplex volume at each iteration. This process is repeated until the desired number of endmembers has been extracted.

It can easily be shown that the MaxD, ATGP, SGA, VCA, and several related algorithms are intrinsically very similar algorithms, but often only differ in their initialization and interpretation. Since the volume of a simplex can be expressed as a product of the volume of one of its faces and the orthogonal distance to this face, maximizing the simplex volume (as done in simplex volume-based algorithms, such as NfindR and SGA) is equivalent to finding the pixel of maximum norm in the orthogonal subspace (as done in VCA, MaxD, ATGP, and related algorithms). This was already observed in [11], and recently, a detailed overview comparing many of these techniques, and highlighting their similarities, appeared in [16].

While all these geometrical EEAs are based on the linear mixing assumption, it is known for a long time that nonlinear spectral mixing may be present in many situations, such as intricate mineral mixtures [17] or vegetation scenery [18]. Nonlinear unmixing algorithms have recently become an active field of research, and many techniques have appeared to deal with these nonlinearities [19], [20].

Another well-known problem in hyperspectral image processing is the intrinsic correlation present in spectra: neighboring spectral bands often show very large correlations, which causes the pixels to lie in a relatively small region of the high-dimensional spectral space, since the spectral axes are not fully independent. This can have an effect on the functioning of algorithms based on the geometrical interpretation of the LMM, where the simplex description is used.

In this paper, we introduce a new EEA that can deal with several of these problems, within the same framework. It has been observed in several papers that simplex volumes and orthogonal distances can be written in terms of distances instead of Euclidean coordinates [21], [22]. This allows us to formulate a linear EEA in terms of mutual distances between the points, resulting in the distance-MaxD (DMaxD) algorithm. Such a distance-based description allows the use of other distance functions, or metrics, instead of Euclidean distances: the distance function effectively becomes a functional parameter of the unmixing algorithm.

Several interesting distance metrics for hyperspectral unmixing applications are kernel and graph distances, and similarity metrics. Kernel distances are the natural metrics derived from certain kernels, typically used to introduce nonlinearity in otherwise linear algorithms. The use of kernels to handle nonlinearity has been exploited multiple times already in spectral unmixing, e.g., the kernel orthogonal subspace projection algorithm [23], [24] for signal identification, and the kernelized fully constrained least-squares algorithm [25]–[28] for solving the inversion problem. These kernels can be employed in the proposed framework as well, through their induced metrics.

Graph-geodesic distances are metrics defined on a graph structure, e.g., the shortest-path distances over a K-nearest neighbor graph. Such graph distances can be used to perform data-driven nonlinear dimensionality reduction (the ISOMAP algorithm [29]), and have been used for unsupervised nonlinear unmixing as well [22]. Employing such a metric in the proposed framework is analogous to combine nonlinear dimensionality reduction via ISOMAP with linear unmixing.

Furthermore, other types of distance metrics can be introduced to cope with the correlations between the spectral bands. For example, by using the Mahalanobis distance instead of the Euclidean distance, the algorithm will take the covariance of the data into account, which becomes equivalent to performing a whitening preprocessing operation. Other distance measures, such as spectral information divergence (SID) or χ^2-distance, have been shown to be powerful measures of similarity in spectral analysis, and might be more natural metrics for unmixing than the Euclidean distance in spectral space. Also physics-based distance functions [26] can be employed, such as those induced by the Hapke model for intimate mineral mixing [30]. In this model, one assumes the LMM, but in an albedo space instead of the traditional reflectance space. Several bilinear models are invertible, and can be used to compose a metric as well. As an example, we present a metric induced by the recently introduced polynomial post-nonlinear model (PPNM) [31], a flexible and powerful model containing bilinear interactions.

When the endmembers are obtained, the next step in the unmixing chain is to determine the abundance maps of each endmember. Under the assumption of white noise, this becomes a constrained least-squares problem, which is geometrically equivalent to a projection operation onto the proper subset (plane, cone, or simplex, depending on the constraints). Since we are no longer using Euclidean metrics, however, the unmixing algorithm should also take the changed metric into account. This can again be accomplished by rewriting a linear unmixing algorithm in terms of distance geometry, and using the metrics under consideration in the altered algorithm.

A linear unmixing algorithm based on the geometrical interpretation of the unmixing problem is the simplex projection unmixing (SPU) algorithm [32]. As we have shown in previous work, this algorithm can be written completely in terms of mutual distances [33], [34], yielding the distance simplex projection unmixing (DSPU) algorithm, which can be used to perform the unmixing step in the proposed nonlinear unmixing chain.

The contributions in this work are hence twofold: 1) we propose the DMaxD algorithm, a new endmember extraction algorithm based on subsequent orthogonal distance maximization, which can function with different metrics and 2) we investigate the performance of the resulting EEA when employed in conjunction with a distance-based unmixing algorithm, allowing us to assess the use of different metrics in an otherwise linear unmixing chain. This extends our previous work, where a distance-based version of the much slower NFindR algorithm was combined with only graph-geodesic distances.

This paper is organized as follows. In Section II, the MaxD algorithm is explained, and the distance-geometry version is introduced. The relation with the several other algorithms is illustrated. In Section III, we introduce several non-Euclidean metrics, which have a clear interpretation when dealing with unmixing problems. In Section IV, we assess the DMaxD algorithm with several of these metrics on artificial data sets, and in Section V on the Cuprite data set. In Section VI, we demonstrate how these algorithms can be used to reproduce several results available in the literature. Section VII contains conclusion and future work.

II. Geometric EEAs in Distance Geometry

Consider a spectral space $\mathbb{R}^D$ of D dimensions, and a data set $\{\boldsymbol{x}_n\}_{n=1}^N$ consisting of N points, of which M points are endmembers. Typically, one identifies the pixel of largest norm as the first endmember

$$\boldsymbol{e}_1 = \boldsymbol{x}_I, \quad I = \underset{n}{\operatorname{argmax}} ||\boldsymbol{x}_n||_2. \tag{2}$$

To find the next endmembers, several strategies can be employed. The SGA adds endmembers by iteratively growing a simplex: let there be q endmembers already identified, with $q < M$. Endmember $q+1$ is identified as that point that maximizes the q-dimensional volume of the simplex spanned by these q endmembers and the candidate endmember

$$\boldsymbol{e}_{q+1} = \boldsymbol{x}_I, \quad I = \underset{n}{\operatorname{argmax}}\, V(\boldsymbol{e}_1, \ldots, \boldsymbol{e}_q, \boldsymbol{x}_n) \tag{3}$$

with $V(\cdot)$ as the volume of the simplex spanned by its arguments. While this volume can be calculated in several ways, we adopt the distance-based version presented in previous work [22]. Consider the squared distance matrix $\boldsymbol{D}_q = \{d_{ij}\}_{i,j=1}^q$, with $d_{ij} = ||\boldsymbol{x}_i - \boldsymbol{x}_j||_2^2$ the squared Euclidean distance between $\boldsymbol{x}_i$ and $\boldsymbol{x}_j$. The volume $V(\boldsymbol{x}_1, \ldots, \boldsymbol{x}_q)$ of the $(q-1)$-simplex spanned by vertices $\{\boldsymbol{x}_1, \boldsymbol{x}_2, \ldots, \boldsymbol{x}_q\}$ can be written in terms of these intervertex distances [35]. This is a multidimensional extension of the formula of Tartaglia for the volume of a tetrahedron

$$(-1)^{q+1} 2^q (q!)^2 V^2 = \det(\boldsymbol{C}_q) \tag{4}$$

where $\boldsymbol{C}_q$ is the Cayley–Menger (CM) matrix of the q points

$$\boldsymbol{C}_q = \begin{bmatrix} \boldsymbol{D}_q & \mathbf{1} \\ \mathbf{1}^T & 0 \end{bmatrix} \tag{5}$$

$$= \begin{bmatrix} 0 & d_{1,2} & \ldots & d_{1,q-1} & d_{1,q} & 1 \\ \vdots & & & \ddots & \vdots & \\ d_{q,1} & d_{q,2} & \ldots & d_{q,q-1} & 0 & 1 \\ 1 & 1 & \ldots & 1 & 1 & 0 \end{bmatrix}. \tag{6}$$

A useful property can be found by introducing the vector $\boldsymbol{d}_q = (d_{1,q}, \ldots, d_{q-1,q}, 1)$. We can write the determinant of $\boldsymbol{C}_q$ as

$$\det(\boldsymbol{C}_q) = -\left(\boldsymbol{d}_q^{\mathrm{T}} \boldsymbol{C}_{q-1}^{-1} \boldsymbol{d}_q\right) \det(\boldsymbol{C}_{q-1}) \tag{7}$$

Algorithm 1. DMaxD

input : Data set $\{\boldsymbol{x}_n\}_{n=1}^N$, number of endmembers M, distance function $D(.,.)$
output: Index set of the endmembers I

```
1  begin
2      I = {argmax_n D(0, x_n)} ;
3      for n = 1, ..., N do
4          d(1, n) = D(x_{I(1)}, x_n)
5      for q = 2, ..., M do
6          P = C(I)^{-1} ;
7          for n = 1, ..., N do
8              v = [d(:, n); 1] ;
9              o(n) = v^T P v ;
10         I = I ∪ {argmax_n o(n)} ;
11         for n = 1, ..., N do
12             d(q, n) = D(x_{I(q)}, x_n);
13     return I
14 end
```

with $\boldsymbol{C}_{q-1}$ the CM matrix of the set $\{\boldsymbol{x}_1, \boldsymbol{x}_2, \ldots, \boldsymbol{x}_{q-1}\}$. This holds true for any permutation of the $(1, 2, \ldots, q)$ indices. This equation states the relation between the simplex volume, and the product of a face volume and the orthogonal distance to this face, and can be used to derive an orthogonal projection operator in terms of mutual distances. The squared orthogonal distance $d_\perp(\boldsymbol{x}_q; \boldsymbol{x}_1, \ldots, \boldsymbol{x}_{q-1})$ from $\boldsymbol{x}_q$ to the hyperplane through the points $(\boldsymbol{x}_1, \ldots, \boldsymbol{x}_{q-1})$ is given by

$$d_\perp(\boldsymbol{x}_q; \boldsymbol{x}_1, \ldots, \boldsymbol{x}_{q-1}) = \frac{\boldsymbol{d}_q^{\mathrm{T}} \boldsymbol{C}_{q-1}^{-1} \mathbf{d}_q}{2}. \tag{8}$$

Hence, the point of maximal orthogonal distance to the hyperplane through the already selected endmembers will also be the point that maximizes the simplex volume, an observation also exploited in the MaxD algorithm [11]. This result can be used to demonstrate the relation between the MaxD, SGA, ATGP, and the VCA algorithms: maximizing the simplex volume and maximizing the orthogonal distance is the same operation.

With these equations, we can now define the distance-geometry maximal distance (DMaxD) algorithm. Let I be an index set $I = (i_1, \ldots, i_q)$, $i_j \in [1, \ldots, N]$. Let the notation $\boldsymbol{C}(I)$ be shorthand for $\boldsymbol{C}_q(\boldsymbol{x}_{I_1}, \ldots, \boldsymbol{x}_{I_q})$, which is the CM matrix of the points indexed by I, and let the distance function $D(\boldsymbol{x}, \boldsymbol{y})$ return the quadratic distance between $\boldsymbol{x}$ and $\boldsymbol{y}$. The DMaxD algorithm is then given in Algorithm 1.

Line 2 determines the first endmember as the endmember farthest from the origin. Lines 3 and 4 calculate the distances from this endmember to all other pixels, and store these as a single row in the distance matrix d. Line 5 starts the main loop that will add $M-1$ additional endmembers iteratively. Lines 6–9 calculate the orthogonal distances from each point $\boldsymbol{x}_n$ to the subspace through the endmember set. The index corresponding to the highest orthogonal distance is added to the endmember index set I in line 10, and the distance matrix d, containing the distances from the current endmember set to all

other data points, is updated in lines 11 and 12. Finally, the resulting endmember index set I is returned in line 13.

Once the endmembers are determined, we need to find the abundances of each endmember in each pixel. In order to use the different metrics, a distance-geometry based unmixing algorithm should be used. The recently introduced SPU algorithm [22] can be rewritten in terms of distances [34], and we refer to this reference for a detailed explanation on how distance-based fully constrained unmixing can be carried out.

Note that both the endmember extraction and the unmixing algorithm are based on the simplex description underlying the LMM, but now extended due to the inherent nonlinearities imposed by the different metrics. This simplex description assumes the presence of both the positivity and sum-to-one constraint, and we implicitly assume that these constraints are also present when other metrics are used. For every metric used in the experimental section, it can be argued that these constraints should indeed be present. In other scenarios, it is possible to relax the sum-to-one constraint to a sum-less-than-one constraint by inclusion of an artificial shade endmember.

III. Metrics

The DMaxD algorithm for endmember extraction and the DSPU algorithm for unmixing both depend on the metric. While an infinite number of metrics exist, several of them are useful when one considers the unmixing problem. In this work, we consider the graph-geodesic distance function, which allows for unsupervised unmixing, the metric induced by the Hapke model for intimate mineral mixtures, the Mahalanobis distance function which corresponds to whitening the data, and the metric induced by the PPNM [31]. As a baseline, we also included the Euclidean metric, resulting in a linear unmixing chain based on MaxD as EEA and SPU as unmixing algorithm.

In this work, we restricted ourselves to metrics, which have a clear meaning in the context of spectral unmixing. Many other metrics can be used as well, and some of these show promising results, e.g., the earth mover's distance or SID. Furthermore, since any kernel function leads to a distance function, kernels can be used as well, and kernel distances are but a subset of the possible metrics that can be used.

Note that the DMaxD algorithm only requires the distances from the current set of endmembers to all other data points, greatly reducing the number of calculations and the memory required by the algorithm. At each iteration, only the distances from the newly added endmember to all other points need to be calculated. This results in a total of $M \times N$ mutual distances that need to be calculated and stored. The computational complexity of the algorithm hence scales linearly in the number of data points N, at least for simple metrics (a counter-example is the graph-geodesic metric, where a distance calculation becomes more involved as N rises). This becomes especially important when using computationally expensive metrics, such as graph-geodesic metrics or the single scattering albedo (SSA) distance.

Note that several of these metrics depend on some intrinsic parameters, with possible additional constraints. In all situations, we assume that these parameters are known and fixed, as opposed to several other strategies employing these mixing models, where the parameters are different for each pixel, or optimization strategies are used with respect to these parameters. In certain situations, the proposed methodology could be used with varying metric parameters as well, and some performance measure such as reconstruction error could be used to optimize the unmixing results. We consider such metric learning strategies beyond the scope of the current contribution, and will focus on the performance of the processing chain for fixed metric parameters.

A. Graph-Geodesic Distances

A popular method for tackling nonlinearities in a data cloud in an unsupervised way is by using a metric based on graph-geodesic distances. A graph geodesic is defined as the shortest-distance path between two points along a graph, and the total length of the graph geodesic is taken as the distance between the two points. The graph is typically a K-nearest neighbor graph, where every point is connected to the K neighbors with smallest Euclidean distance, and the weights of the edges are their Euclidean lengths.

A K-nearest neighbor graph can be efficiently calculated using GPU implementations [36], and graph geodesics and their lengths can be easily determined with the Dijkstra algorithm [37]. The complete distance matrix can in theory be calculated beforehand. The graph metric depends on the connectivity parameter K. We do not aim to investigate the dependence on this parameter in this work, and choose $K = 10$ for all experiments involving the graph metric. Using a graph-geodesic distance in the proposed framework is comparable to performing a nonlinear dimensionality reduction through the ISOMAP algorithm [29] before executing a linear unmixing chain.

B. Mahalanobis Distance

The Mahalanobis distance is a dissimilarity measure that takes the distribution of the data into account. Along each principal component axis, the distances are rescaled with the corresponding standard deviation. This is accomplished by taking the covariance of the data into account in the distance function

$$d(\boldsymbol{x}, \boldsymbol{y}) = (\boldsymbol{x} - \boldsymbol{y})^T \boldsymbol{Z}^{-1} (\boldsymbol{x} - \boldsymbol{y}) \tag{9}$$

with $\boldsymbol{Z}$ is the data covariance matrix. Using the Mahalanobis distance in the DMaxD algorithm corresponds to whitening the data before executing the MaxD algorithm. Especially in hyperspectral data sets, large correlations can be expected between adjacent spectral bands, and by using Mahalanobis distances, the effects of such correlations can be alleviated. It must be noted that in certain hyperspectral data sets, the inversion of the covariance matrix might be unstable, and using this type of metric might yield unsatisfactory results.

C. SSA Distance

A popular model for describing the optical effects in particulate media is the isotropic multiple scattering approximation model proposed in [30], also known as the Hapke model.

This model is also a LMM, but in terms of SSA instead of reflectance. To convert a reflectance x_d in the vector $\boldsymbol{x} = (x_1, \ldots, x_D)$ to its corresponding SSA w_d one can use the relation

$$\sqrt{1 - w_d} = \frac{\left[(\mu_0 + \mu)^2 x_d^2 + (1 + 4\mu_0\mu x_d)(1 - x_d)\right]^{\frac{1}{2}} - (\mu_0 + \mu)x_d}{1 + 4\mu_0\mu x_d} \tag{10}$$

where variables μ and μ_0 are the cosines of the angles with the normal of the incoming and outgoing radiation, respectively. This model can hence be employed in the proposed distance-geometric framework as well, by considering Euclidean distances in SSA space instead of reflectance space

$$d(\boldsymbol{x}, \boldsymbol{y}) = ||\boldsymbol{w}_x - \boldsymbol{w}_y||_2^2 \tag{11}$$

with $\boldsymbol{w}_x$ and $\boldsymbol{w}_y$ are the SSA vectors associated with $\boldsymbol{x}$ and $\boldsymbol{y}$, respectively, given by (10). A similar kernel-based approach was presented in [26], and applied in a kernelized fully constrained least-squares unmixing (KFCLSU) algorithm. For an introduction on the use of the Hapke model in hyperspectral unmixing, we refer to [19]. For a detailed derivation of the full Hapke model, we refer to the original paper [30] or the book [38].

D. PPNM Distance

The recently introduced PPNM model is a bilinear model that can be introduced in two different ways: either as a second-degree polynomial transformation of a LMM, or with an explicit bilinear mixing equation. Let x_d and e_{md} be the dth band of $\boldsymbol{x}$ and $\boldsymbol{e}_m$, respectively,

$$x_d = y_d + by_d^2 \tag{12}$$

$$y_d = \sum_{m=1}^{M} a_m e_{md} \tag{13}$$

or

$$\boldsymbol{x} = \sum_{m=1}^{M} a_m \boldsymbol{e}_m + b \sum_{m=1}^{M} \sum_{k=1}^{M} a_m a_k \boldsymbol{e}_m \odot \boldsymbol{e}_k \tag{14}$$

where b is a model parameter which should be larger than -0.5 [31]. If one assumes that a data set can be modeled using the PPNM with a known parameter b, one can employ the proposed unmixing methodology by introducing a PPNM-distance, given by

$$d(\boldsymbol{x}, \boldsymbol{y}) = \frac{1}{4} \left\| \sqrt{1 + 4b\boldsymbol{x}} - \sqrt{1 + 4b\mathbf{y}} \right\|_2^2. \tag{15}$$

This distance function can be obtained by inverting the mixing (12) and calculating the Euclidean distance. Remark that a constant known value of b is assumed for the entire scene, as opposed to the unmixing strategy in [31], where the nonlinearity parameter b can vary on a per-pixel basis, allowing more flexibility. On the other hand, the techniques proposed in [31] are only used for solving the inversion or unmixing step, whereas the proposed methodology can also extract endmembers taking the mixing model into account.

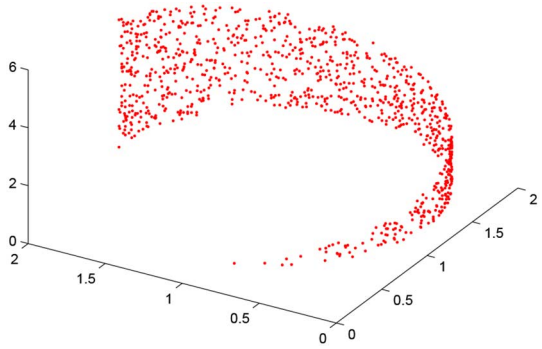

Fig. 1. Toy data set.

IV. Artificial Data

A. Setup of the Experiment

To assess the DMaxD algorithm, and unmixing using different metrics in general, we first employ synthetic data sets since in such data sets the endmembers, abundances, and noise vectors are known exactly. The endmembers are randomly selected from the USGS mineral database, and the abundances are chosen randomly and uniformly from a unit simplex. The data sets are then generated using

1) the LMM;
2) the PPNM model (12) with $b = 1$;
3) the Hapke model for intimate mixing, where the reflectance values are converted to SSA, linearly mixed using the abundances, and then converted back to reflectances.

The number of data points is 10^4 and the number of endmembers is $M = 5$. Furthermore, a toy data set composed of a two-dimensional (2-D) simplex wrapped on a cylinder is employed as well. This data set is depicted in Fig. 1 and contains 1000 points. Optionally, random Gaussian noise with a known signal-to-noise ratio (SNR) is added, and we made sure that every endmember is present in each data set as a noiseless pure pixel. Note that we used $K = 10$ for the graph-geodesic metric, $b = 1$ for the PPNM metric, and $\mu = 1$ and $\mu_0 = 0.5$ for the Hapke metric in all experiments. In this work, we do not aim at investigating the effects of these parameters, but ideally, an optimization with respect to these parameters could be carried out.

To assess the endmember extraction performance of the DMaxD algorithm, the spectral angles between the obtained and known endmembers are calculated, the best match retained for each endmember, and averaged over all endmembers. The unmixing step with the SPU algorithm is assessed by calculating the mean absolute differences between the known and obtained abundances, where the correct noiseless endmembers were used to perform the unmixing.

B. Endmember Extraction

The average spectral angles between the endmembers obtained by the DMaxD algorithm and the known endmembers are listed in Table I for noiseless data, and in Table II, for the same data sets, but with noise with $\mathrm{SNR} = 25$ present. From

TABLE I
AVERAGE SPECTRAL ANGLE, AVERAGED OVER 100 RUNS, FOR SEVERAL NOISELESS DATA SETS AND METRICS

Metrics	Linear	Hapke	PPNM	Toy
Linear	**0.0000**	0.0057	0.0007	0.2319
Hapke	0.0181	**0.0000**	0.0318	0.1505
Graph $K = 10$	0.0128	0.0161	0.0165	**0.0000**
Mahalanobis	0.0178	0.0164	0.0068	0.2015
PPNM	0.0001	0.0037	**0.0000**	0.2292

The best result is indicated in bold.

TABLE II
AVERAGE SPECTRAL ANGLE, AVERAGED OVER 100 RUNS, FOR SEVERAL DATA SETS AND METRICS

Metrics	Linear	Hapke	PPNM	Toy
Linear	0.0060	0.0097	0.0058	0.2466
Hapke	0.0194	0.0088	0.0335	0.2734
Graph $K = 10$	0.0256	0.0320	0.0324	**0.0016**
Mahalanobis	0.0358	0.0411	0.0394	0.2046
PPNM	**0.0051**	**0.0073**	**0.0040**	0.2444

Noise with $\mathrm{SNR} = 25$ was added. The best result is indicated in bold.

TABLE III
AVERAGE ABSOLUTE ABUNDANCE DIFFERENCES, AVERAGED OVER 100 RUNS, FOR SEVERAL NOISELESS DATA SETS AND METRICS

Metrics	Linear	Hapke	PPNM	Toy
Linear	**0.0000**	0.1097	0.0321	0.0924
Hapke	0.1163	**0.0000**	0.2357	0.2092
Graph $K = 10$	0.1754	0.1486	0.1727	**0.0499**
Mahalanobis	0.1508	0.1958	0.1431	0.1604
PPNM	0.0213	0.0998	**0.0000**	0.1181

The best result is indicated in bold.

these tables, it is clear that when the mixing model is known, using the corresponding metric in the DMaxD algorithm will always yield the correct endmember set in the absence of noise. Another observation is that the graph-geodesic metric is the only one capable of dealing with uncommon mixing scenarios such as depicted in the toy data set. Furthermore, it is worth noting that the PPNM metric performs well on most data sets regardless of the mixing model. Especially, when noise is present, the PPNM outperforms all other metrics in the endmember extraction task. This robustness was already claimed in [31] and seems to be confirmed by these results. Finally, the Mahalanobis distance is outperformed by most metrics on most data sets, suggesting that the data whitening might have a negative effect on the endmember extraction capabilities.

C. Unmixing Performance

When the correct endmembers are used in the SPU algorithm with the various metrics, the average absolute abundance differences listed in Tables III and IV are obtained, for the noiseless and noisy case, respectively. Also here, the use of the correct metric results in perfect unmixing results, at least in the absence of noise. The unmixing results obtained by the graph-geodesics outperform the other metrics only on the toy data set. Again, it can be observed that the PPNM metric will yield decent results for most data sets.

TABLE IV
AVERAGE ABSOLUTE ABUNDANCE DIFFERENCES, AVERAGED OVER 100 RUNS, FOR SEVERAL DATA SETS AND METRICS

Metrics	Linear	Hapke	PPNM	Toy
Linear	**0.0234**	0.1344	0.0584	0.0951
Hapke	0.1159	**0.0432**	0.1951	0.2046
Graph $K = 10$	0.1545	0.1949	0.1669	**0.0483**
Mahalanobis	0.0256	0.1571	0.0667	0.1590
PPNM	0.0300	0.1217	**0.0501**	0.1183

Noise with $\mathrm{SNR} = 25$ was added. The best result is indicated in bold.

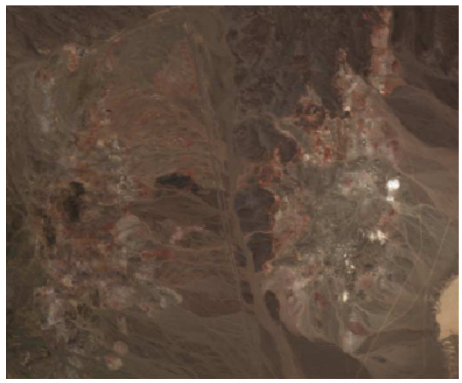

Fig. 2. AVIRIS Cuprite data set, in approximated true colors.

V. DEMONSTRATION ON CUPRITE DATA SET

Both the endmember extraction and unmixing steps have been carried out on the well-known AVIRIS Cuprite data set as well, depicted in Fig. 2. While the minerals that are present in this data set are relatively well-known, no abundance ground truth is available, and unfortunately one cannot make any quantitative assessment of the unmixing results. Furthermore, the Cuprite data set is used very often to evaluate linear unmixing techniques, but it is not entirely clear that the LMM is indeed the most appropriate mixing model for this data set. On the contrary, in [39], it is already shown that non-LMMs, i.e., the Hapke model, might be more appropriate for unmixing spectra observed in certain areas of the Cuprite mining district. Hence, while we cannot compare abundance maps with any ground truth due to its nonexistence, it is not unreasonable to assume that abundance maps obtained by different mixing models might be more appropriate.

A. Endmember Extraction

The first step is to execute the DMaxD algorithm to extract endmembers. We chose to extract 10 endmembers, which are shown in Fig. 3 for each of the introduced metrics.

It can be seen from these spectra that the introduction of different metrics can have a large effect on the retrieved endmembers, although some common spectra are present in each endmember set as well. Identification of these endmembers can be done by locating the spectrum in the USGS spectral database with smallest spectral angle.

These identified minerals are listed in Table V. For each metric and mineral, we list how many times that mineral was the

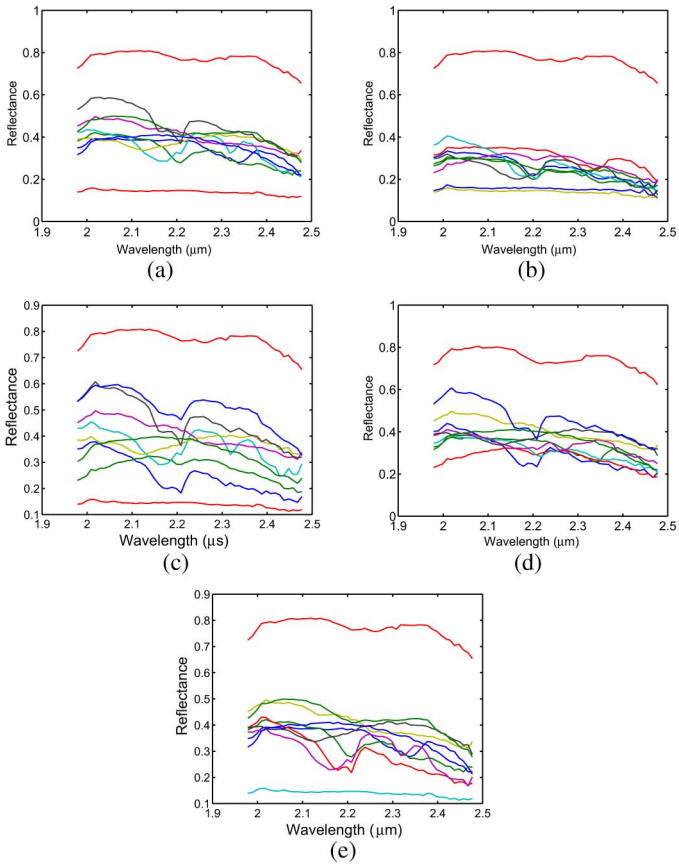

Fig. 3. Endmembers retrieved with the DMaxD algorithm, for several metrics. (a) Linear, (b) Hapke, (c) Graph $K = 10$, (d) Mahalanobis, and (e) PPNM.

TABLE V
MINERALS IDENTIFIED FOR EACH METRIC

Mineral	Linear	Graph	Mahal.	Hapke	PPNM
Alunite	1	2		1	1
Beryl	1	1		2	1
Chert	2	1	1	1	2
Hydrogros.	1			1	1
Kaolinite	1	2	2	1	1
Mizzonite	1	1		1	1
Mordenite	1	1	2	1	1
Orthoclase	1	1	1		1
Zoisite	1		1	1	1
Other		1	3	1	

best fit with a retrieved endmember. We grouped the different physical configurations of minerals together. For example, there are 17 different spectra corresponding to kaolinite in the USGS database, and if two endmembers are identified with any of these, there will be a number 2 in the table. The number 0 is not shown for clarity. Minerals that appear only once in a row are grouped together in the "other" category.

From this table, it is clear that several minerals that are known to be present in the Cuprite data set in large quantities, such as alunite, kaolinite, or beryl, are retrieved by every metric except the Mahalanobis metric. The other retrieved minerals show some differences, but several of these are known to be present in the Cuprite data set as well.

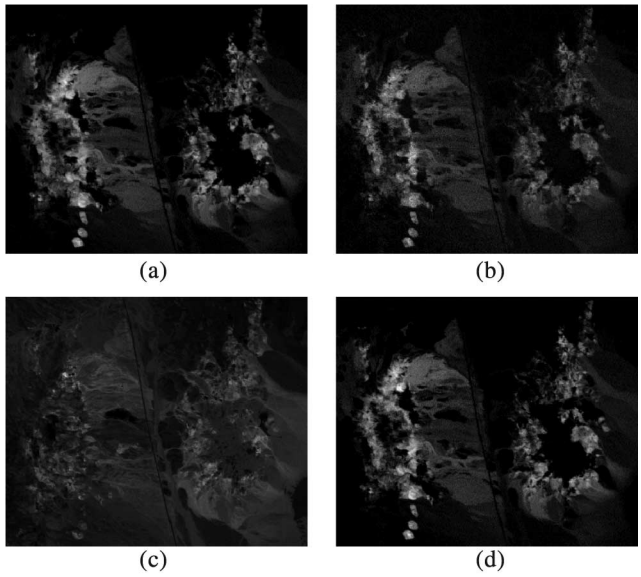

Fig. 4. Abundance maps of the alunite endmember, for the metrics used. No alunite endmember was identified for the Mahalanobis distance. (a) Linear, (b) Hapke, (c) Graph $K = 10$, and (d) PPNM.

B. Abundance Maps

Once the endmembers have been determined, we can use them in the DSPU algorithm to obtain the abundance maps, respecting the employed metrics. To avoid plotting a high number of abundance maps, we only present the abundance maps for two well-known minerals in the Cuprite data set, i.e., alunite (Fig. 4) and kaolinite (Fig. 5). If one of these endmembers is identified more than once, the presented abundance map is the sum of the abundance maps of each endmember. If one of the minerals is not present in the extracted endmember sets, it is indicated as well.

Unfortunately, since no ground truth is available on the abundance level, we cannot discuss these results quantitatively, and only qualitative assessment is possible. Most of the metrics result in abundance maps that are visually similar to the linear abundance maps. The graph and Mahalanobis distance seem to show a larger differences with the linear map. We can conclude that several of these metrics will result in abundance maps, which differ slightly from those obtained with a linear unmixing chain, and due to the inherent nonlinearities built in through the metrics, can be very useful tools for exploring nonlinear mixing effects in hyperspectral imagery. Several nonlinear unmixing methods and preprocessing techniques can be used in the proposed unmixing framework through the use of the proper metric. Because currently no hyperspectral data sets are available that show nonlinear effects and have detailed ground truth available, we are unable to quantitatively assess the proposed unmixing chain.

From a computational point of view, the nonlinear unmixing chain is very competitive with respect to several nonlinear alternatives. The runtime of the MATLAB implementation of the DMaxD algorithm varies from 17 s for the linear metric to 260 s for the graph-geodesic metric, when executed on the Cuprite data set with 109 865 pixels and $M = 10$ endmembers,

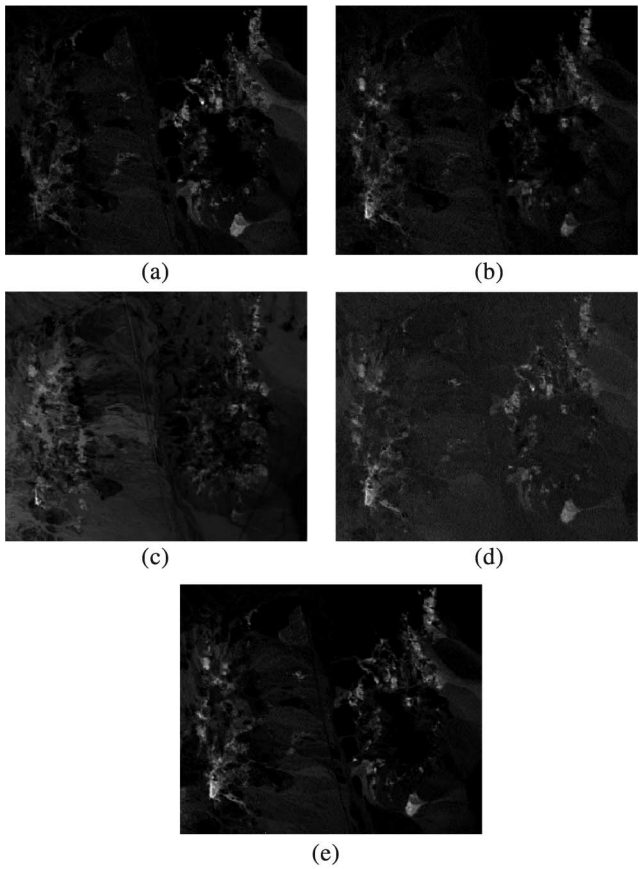

Fig. 5. Abundance maps of the kaolinite endmember, for the metrics used. (a) Linear, (b) Hapke, (c) Graph $K = 10$, (d) Mahalanobis, and (e) PPNM.

on a single core of a I7 processor at 3.6 GHz. The runtime of the DSPU algorithm is similar for all metrics used, and is around 8 s.

VI. Benchmark Tests

Finally, we can compare the unmixing performance for some of these metrics with results present in the literature, as several of these metrics will result in a processing chain that shows great similarity to existing techniques.

The use of the graph-geodesic distances yields a chain comparable to the one presented recently in [34], with the exception that the proposed EEA is based on the MaxD algorithm, while in [34] the EEA is based on NFindR [2]. The unmixing step for obtaining the abundances is identical.

To assess this similarity, we have compared the endmembers extracted from the Cuprite data set [Fig. 3 (c)] with those obtained with the NFindR-based technique from [34] when using the same KNN graph with $K = 10$. Four out of ten obtained endmembers were identical, whereas seven out of ten endmembers were identified with the same minerals, indicating that very similar results are obtained with either method.

When one uses the SSA distance based on the Hapke model, the unmixing step of the processing chain should become identical to unmixing with the Hapke model, as performed in many papers [26], [40], [41], and [19]. Many results using this model are available in the literature, and as a benchmark, we can reproduce some of them. We refer to [30] for the theory behind the Hapke model, and to [40] and [42] for a detailed explanation of the unmixing procedure based on this model, and the used assumptions and simplifications. Note that this approach assumes that the endmembers are known and hence we can only test the unmixing phase of the chain.

TABLE VI
Abundance of Quartz in a Quartz–Alunite Binary Mixture, the Abundances Obtained by Unmixing Via the Hapke Method, and the DSPU Algorithm Employing the Hapke Metric

Abundance	1	0.75	0.5	0.25	0
Hapke unmixing	1.0000	0.7210	0.4966	0.2466	0
DSPU	1.0000	0.7210	0.4966	0.2466	0

We unmixed spectra of mixtures of quartz and alunite with different abundance ratios. The spectra are available in the RELAB spectral database and are described in detail in [43]. In Table VI, we listed the results obtained by using the Hapke model and the DSPU algorithm using the Hapke metric. Both results are indiscernible, as the average difference between the obtained abundances are 7×10^{-7}. This indicates the equivalence between both methods.

Yet another comparison can be made between the proposed DSPU unmixing step, and KFCLSU [25]–[28]. As a kernel function $\kappa(\boldsymbol{x}, \boldsymbol{y})$ describes an inner product in some feature space, it can be used to define a distance function as well

$$d(\boldsymbol{x}, \boldsymbol{y}) = \kappa(\boldsymbol{x}, \boldsymbol{x}) + \kappa(\boldsymbol{y}, \boldsymbol{y}) - 2\kappa(\boldsymbol{x}, \boldsymbol{y}). \tag{16}$$

Hence, using this distance function in the DSPU algorithm will create an algorithm that is equivalent to using the associated kernel function in the KFCLSU algorithm. This can be demonstrated by implementing the KFCLSU algorithm as described in [25] and unmixing a data set with both methods, yielding identical results.

VII. Conclusion

We have presented a nonlinear unmixing chain, containing an endmember extraction and unmixing algorithm written in terms of distance geometry. The introduced DMaxD algorithm is based on the MaxD algorithm and uses subsequent orthogonal distance maximization to identify the endmembers. The relation with several other EEAs, such as the SGA, ATGP, and the VCA algorithm, is demonstrated, and a compact, efficient implementation of the DMaxD algorithm is provided. After the endmembers have been extracted, the DSPU algorithm can be employed to obtain the abundance maps.

Since both these algorithms are written in distance geometry, other metrics can be introduced, and several nonlinearities or preprocessing steps can be handled through these metrics. A common technique for introducing nonlinearities is the kernel trick, which can also be applied here through the introduction of kernel distances. Graph-geodesic distances simulate the use of nonlinear dimensionality reduction, while using the Mahalanobis distance is equivalent to executing a whitening preprocessing step. Several other useful metrics can be used as well, such as those based on certain physical models as the Hapke model for intimate mixtures or bilinear models such as the PPNM.

The endmember extraction and unmixing capabilities of this processing chain is demonstrated quantitatively on simulated data sets, and a real experiment on the AVIRIS Cuprite data set is performed as well. The obtained endmembers are presented, and an identification table provided. Next, the abundance maps for two well-known minerals present in the Cuprite data set, i.e., alunite and kaolinite, are presented for the used metrics. It is shown that most of these metrics will yield abundance maps that show subtle differences with the linear abundance maps. These results suggest that this approach for nonlinear unmixing can be a very promising path to be explored and can give very decent unmixing results if the correct metrics are used.

Future work consists in testing the unmixing chain on data sets where the ground truth is known, and on data sets that show large nonlinearities. Other metrics could be introduced and investigated as well. Furthermore, several metrics depend on parameters that are *a priori* unknown, and optimization with respect to such parameters can be investigated.

REFERENCES

[1] N. Keshava and J. F. Mustard, "Spectral unmixing," *IEEE Signal Process. Mag.*, vol. 19, no. 1, pp. 44–57, Jan. 2002.

[2] M. E. Winter, "N-FINDR: An algorithm for fast autonomous spectral end-member determination in hyperspectral data," *Proc. SPIE*, vol. 3753, pp. 266–275, 1999.

[3] P. J. Martínez *et al.*, "Endmember extraction algorithms from hyperspectral images," *Ann. Geophys.*, vol. 49, no. 1, pp. 93–101, Feb. 2006.

[4] M. Zortea and A. Plaza, "A quantitative and comparative analysis of different implementations of N-FINDR: A fast endmember extraction algorithm," *IEEE Geosci. Remote Sens. Lett.*, vol. 6, no. 4, pp. 787–791, Oct. 2009.

[5] C.-I. Chang, C.-C. Wu, and C. T. Tsai, "Random N-finder (N-FINDR) endmember extraction algorithms for hyperspectral imagery," *IEEE Trans Image Process.*, vol. 20, no. 3, pp. 641–656, Mar. 2011.

[6] W. Xiong, C.-I. Chang, C.-C. Wu, K. Kalpakis, and H.-M. Chen, "Fast algorithms to implement N-FINDR for hyperspectral endmember extraction," *IEEE J. Sel. Topics Appl. Earth Obs. Remote Sens.*, vol. 4, no. 3, pp. 545–564, May 2011.

[7] A. Plaza and C.-I. Chang, "Impact of initialization on design of endmember extraction algorithms," *IEEE Trans. Geosci. Remote Sens.*, vol. 44, no. 11, pp. 3397–3407, Nov. 2006.

[8] C.-C. Wu, H.-M. Chen, and C.-I. Chang, "Real-time N-finder processing algorithms for hyperspectral imagery," *J. Real-Time Image Process.*, vol. 7, no. 2, pp. 105–129, 2012.

[9] S. Dowle, R. Takashima, and M. Andrews, "Reducing the complexity of the N-FINDR algorithm for hyperspectral image analysis," *IEEE Trans. Image Process.*, vol. 22, no. 7, pp. 2835–2848, Sep. 2012.

[10] S. Sanchez, G. Martín, and A. Plaza, "Parallel implementation of the N-FINDR endmember extraction algorithm on commodity graphics processing units," *Proc. IEEE IGARSS*, 2010, pp. 955–958.

[11] J. R. Schott, K. Lee, R. V. Raqueno, G. D. Hoffmann, and G. Healey, "A subpixel target detection technique based on the invariance approach," *Proc. Airborne Visible InfraRed Imag. Spectrometer (AVIRIS) Workshop*, 2003.

[12] H. Ren and C.-I. Chang, "Automatic spectral target recognition in hyperspectral imagery," *IEEE Trans. Aerosp. Electron. Syst.*, vol. 39, no. 4, pp. 1232–1249, Oct. 2003.

[13] J. M. P. Nascimento and J. M. Bioucas-Dias, "Vertex component analysis: A fast algorithm to unmix hyperspectral data," *IEEE Trans. Geosci. Remote Sens.*, vol. 43, no. 4, pp. 898–910, Apr. 2005.

[14] X. Tao, B. Wang, and L. Zhang, "A new approach to decomposition of mixed pixels based on orthogonal bases of data space," *Lect. Notes Comput. Sci.*, vol. 4681, pp. 1029–1040, 2007.

[15] C.-I. Chang, C.-C. Wu, W.-M. Liu, and Y.-C. Ouyang, "A new growing method for simplex-based endmember extraction algorithm," *IEEE Trans. Geosci. Remote Sens.*, vol. 44, no. 10, pp. 2804–2819, Oct. 2006.

[16] W.-K. Ma *et al.*, "A signal processing perspective on hyperspectral unmixing: Insights from remote sensing," *IEEE Signal Process. Mag.*, vol. 31, no. 1, pp. 67–81, Jan. 2014.

[17] D. B. Nash and J. E. Conel, "Spectral reflectance systematics for mixtures of powdered hypersthene, labradorite, and ilmenite," *J. Geophys. Res.*, vol. 79, pp. 1615–1621, 1974.

[18] A. R. Huete, R. D. Jackson, and D. F. Post, "Spectral response of a plant canopy with different soil backgrounds," *Remote Sens. Environ.*, vol. 17, no. 1, pp. 37–53, 1985.

[19] R. Heylen, M. Parente, and P. Gader, "A review of nonlinear hyperspectral unmixing methods," *IEEE J. Sel. Topics Appl. Earth Obs. Remote Sens.*, vol. 7, no. 6, pp. 1844–1868, Jun. 2014.

[20] N. Dobigeon *et al.*, "Nonlinear unmixing of hyperspectral images: Models and algorithms," *IEEE Signal Process. Mag.*, vol. 31, no. 1, pp. 82–94, Jan. 2014.

[21] X. Zhang, X.-H. Tong, and M.-L. Liu, "An improved N-FINDR algorithm for endmember extraction in hyperspectral imagery," in *Proc. 2009 Joint Urban Remote Sens. Event*, 2009, pp. 1–5.

[22] R. Heylen, D. Burazerović, and P. Scheunders, "Non-linear spectral unmixing by geodesic simplex volume maximization," *IEEE J. Sel. Topics Signal Process.*, vol. 5, no. 3, pp. 534–542, Oct. 2011.

[23] H. Kwon and N. Nasrabadi, "Kernel orthogonal subspace projection for hyperspectral signal classification," *IEEE Trans. Geosci. Remote Sens.*, vol. 43, no. 12, pp. 2952–2962, Dec. 2005.

[24] B. Wu, L. Zhang, P. Li, and J. Zhang, "Nonlinear estimation of hyperspectral mixture pixel proportion based on kernel orthogonal subspace projection," *Adv. Neural Netw.*, vol. 3971, pp. 1070–1075, 2006.

[25] B. Broadwater, R. Chellappa, A. Banerjee, and P. Burlina, "Kernel fully constrained least squares abundance estimates," *Proc. IEEE IGARSS*, 2007, pp. 4041–4044.

[26] J. Broadwater and A. Banerjee, "A comparison of kernel functions for intimate mixture models," in *Proc. IEEE Workshop Hyperspectral Image Signal Process. Evolut. Remote Sens. (WHISPERS)*, 2009, pp. 1–4.

[27] J. Broadwater and A. Banerjee, "A generalized kernel for areal and intimate mixtures," in *Proc. IEEE Workshop Hyperspectral Image Signal Process. Evolut. Remote Sens. (WHISPERS)*, 2010, pp. 1–4.

[28] J. Broadwater and A. Banerjee, "Mapping intimate mixtures using an adaptive kernel-based technique," *Proc. IEEE Workshop Hyperspectral Image Signal Process. Evolut. Remote Sens. (WHISPERS)*, 2011, pp. 1–4.

[29] J. B. Tenenbaum, V. de Silva, and J. C. Langford, "A global geometric framework for nonlinear dimensionality reduction," *Science*, vol. 290, no. 5500, pp. 2319–2323, 2004.

[30] B. Hapke, "Bidirectional reflectance spectroscopy. 1. Theory," *J. Geophys. Res.*, vol. 86, pp. 3039–3054, 1981.

[31] Y. Altmann, A. Halimi, N. Dobigeon, and J.-Y. Tourneret, "Supervised nonlinear spectral unmixing using a polynomial post nonlinear model for hyperspectral imagery," in *Proc. IEEE Int. Conf. Acoust. Speech Signal Process. (ICASSP)*, May 2011, pp. 1009–1012.

[32] R. Heylen and P. Scheunders, "Fully constrained least-squares spectral unmixing by simplex projection," *IEEE Trans. Geosci. Remote Sens.*, vol. 49, no. 11, pp. 4112–4122, Jun. 2011.

[33] R. Heylen and P. Scheunders, "Spectral unmixing using distance geometry," in *Proc. IEEE Workshop Hyperspectral Image Signal Process. Evolut. Remote Sens. (WHISPERS)*, 2011, pp. 1–4.

[34] R. Heylen and P. Scheunders, "A distance geometric framework for nonlinear hyperspectral unmixing," *IEEE J. Sel. Topics Appl. Earth Obs. Remote Sens.*, vol. 7, no. 6, pp. 1879–1888, Jun. 2014.

[35] S. Rabinowitz, "The volume of an n-simplex with many equal edges," *Missouri J. Math. Sci.*, vol. 1, pp. 11–17, 1989.

[36] V. Garcia, E. Debreuve, and M. Barlaud, "Fast K nearest neighbor search using gpu," in *Proc. CVPR Workshop Comput. Vis. GPU*, 2008, pp. 1–6.

[37] E. W. Dijkstra, "A note on two problems in connexion with graphs," *Numer. Math.*, vol. 1, pp. 269–271, 1959.

[38] B. Hapke, *Theory of Reflectance and Emittance Spectroscopy*. Cambridge, U.K.: Cambridge Univ. Press, 2005.

[39] H. Shipman and J. B. Adams, "Detectability of minerals on desert alluvial fans using reflectance spectra," *J. Geophys. Res.: Solid Earth*, vol. 92, no. B10, pp. 10391–10402, 1987.

[40] J. F. Mustard and C. M. Pieters, "Quantitative abundance estimates from bidirectional reflectance measurements," *J. Geophys. Res.: Solid Earth*, vol. 92, no. B4, pp. E617–E626, 1987.

[41] J. F. Mustard and C. M. Pieters, "Photometric phase functions of common geologic minerals and applications to quantitative analysis of mineral mixture reflectance spectra," *J. Geophys. Res.: Solid Earth*, vol. 94, no. B10, pp. 13619–13634, 1989.

[42] R. Heylen, P. Scheunders, A. Rangarajan, and P. Gader, "Nonlinear unmixing by using non-euclidean metrics in a linear unmixing chain," in *Proc. IEEE Workshop Hyperspectral Image Signal Process. Evolut. Remote Sens. (WHISPERS)*, 2014, pp. 1–4.
[43] T. Hiroi and C. M. Pieters, "Effects of grain size and shape in modeling reflectance spectra of mineral mixtures," *Proc. Lunar Planet. Sci.*, vol. 22, pp. 313–325, 1992.

Rob Heylen (M'10) received the B.S., M.S., and Ph.D. degrees in physics, with work in the field of statistical mechanics, from the Katholieke Universiteit Leuven, Leuven, Belgium, in 2001, 2003, and 2008, respectively.

In 2009, he became a Postdoctoral Researcher with the IMinds-Vision Lab, Department of Physics, University of Antwerp, Antwerp, Belgium. His research interests include hyperspectral image processing and computational physics. He is a Postdoctoral Fellow of the Research Foundation–Flanders (FWO).

Paul Scheunders (M'98) received the B.S. and Ph.D. degrees in physics, with work in the field of statistical mechanics, from the University of Antwerp, Antwerp, Belgium, in 1983 and 1990, respectively.

In 1991, he became a Research Associate with the Vision Lab, Department of Physics, University of Antwerp, where he is currently a Professor. He has authored/coauthored over 120 papers in international journals and proceedings in the field of image processing and pattern recognition. His research interests include wavelets and multispectral image processing.

Anand Rangarajan received the Ph.D. degree from the University of Southern California, Los Angeles, CA, USA.

He is an Associate Professor with the Department of Computer and Information Science and Engineering, University of Florida, Gainesville, FL, USA. Prior to this, he was an Assistant Professor with the Departments of Diagnostic Radiology and Electrical Engineering, Yale University, New Haven, CT, USA. His research interests include machine learning, computer vision, medical and hyperspectral imaging, and the scientific study of consciousness.

Paul Gader (M'86–SM'09–F'11) received the Ph.D. degree in mathematics for image-processing-related research from the University of Florida, Gainesville, FL, USA, in 1986.

He was a Senior Research Scientist with Honeywell, a Research Engineer and a Manager with the Environmental Research Institute of Michigan, Ann Arbor, MI, USA, and a Faculty Member with the University of Wisconsin, Oshkosh, WI, USA, the University of Missouri, Columbia, MO, USA, and the University of Florida, FL, USA, where he is currently a Professor and the Interim Chair of Computer and Information Science and Engineering. He performed his first research in image processing in 1984 working on algorithms for the detection of bridges in forward-looking infrared imagery as a Summer Student Fellow at Eglin Air Force Base. He has since worked on a wide variety of theoretical and applied research problems including fast computing with linear algebra, mathematical morphology, fuzzy sets, Bayesian methods, handwriting recognition, automatic target recognition, biomedical image analysis, landmine detection, human geography, and hyperspectral and light detection, and ranging image analysis projects. He has authored/co-authored hundreds of refereed journal and conference papers.